Overirradiance: caracterization and forecast in the central Amazon

Vinicius Roggério da Rocha[1] , Rodrigo Santos Costa[1], Gilberto Fisch[12], António Ruano[34]

[1] INPE - National Institute for Space Research, São José dos Campos - SP (Brazil)

[2] UNITAU – Universidade de Taubaté – SP (Brazil)

[3] UALG - University of Algarve, Faro (Portugal)

[4] IDMEC - Instituto Superior Técnico, Universidade de Lisboa, Lisboa (Portugal)

Abstract

In this study, we present some aspects related with the relationship between overirradiance, short-term irradiance variability and cloud cover in Central Amazonia. The analysis focuses on how cloud morphology and atmospheric conditions modulate the temporal structure of surface solar irradiance. Results show a positive correlation (r = 0.63) was found between DARR and overirradiance frequency, stronger during the wet season (r = 0.67) than the dry season (r = 0.58), reflecting the role of fragmented cloud fields and optical properties in enhancing rapid fluctuations. Intraday variability peaks around local noon, particularly in the afternoon, indicating higher susceptibility to sharp irradiance ramps during this period. Cloud type analysis shows that low clouds dominate overirradiance events, while *cirrus* and *altocumulus* also increase in frequency, though with lower optical efficiency. *Cumulus congestus* and low clouds produce the most intense ramps, whereas *cirrus* generate lower but still significant fluctuations. These results highlight the influence of cloud morphology on the temporal structure of solar irradiance and provide a physical basis to support very short-term forecasting approaches, as discussed in Rocha et al. (2025) e Rocha (2025).

Keywords: surface solar irradiance, cloud enhancement, solar variability, cloud types, GHI, prediction

1. Introduction

The expansion of solar energy has consolidated itself as one of the main drivers of the global energy transition, propelled by technological advances and the growing demand for renewable and decentralized sources. In Brazil, the installed capacity of photovoltaic generation increased more than fortyfold between 2017 and 2024, reaching approximately 23% of the national electricity matrix (ABSOLAR, 2025). Despite this progress, challenges persist in tropical regions such as the Amazon, where high cloudiness and the complexity of atmospheric processes impose limitations and uncertainties on the integration of solar energy into power systems (Pereira et al., 2017; REN21, 2025).

The variability of solar irradiance - resulting from the combination of astronomical factors and meteorological conditions - represents one of the main obstacles to the safe and efficient operation of photovoltaic systems. At hourly and sub-hourly scales, rapid fluctuations associated with cloud passages are particularly critical, potentially causing abrupt drops or sharp peaks in irradiance. Among these extreme events, overirradiance stands out, characterized by values exceeding the theoretical maximum expected under clear-sky conditions, with the potential to affect inverters and other components of the electrical grid. Anticipating such events is essential for protection strategies and operational optimization, especially in highly variable regions such as Central Amazonia.

Several studies have advanced the development of very short-term irradiance forecasting models, including approaches based on machine learning. However, understanding the meteorological mechanisms and variability patterns associated with overirradiance is equally important for improving these models and guiding their application in regional energy planning. In particular, cloud types and morphological properties play a central role in these processes by modulating, in distinct ways, the occurrence and intensity of overirradiance events.

10.18086/swc.2025.04.35 Available at http://proceedings.ises.org

In tropical regions, the temporal variability of cloud cover is high, with a predominance of convective processes that are difficult to predict (Laing and Evans, 2011). This dynamic generates rapid and intense fluctuations in Global Horizontal Irradiance at the surface (GHI), on timescales ranging from minutes to hours. The spatial andtemporal variation of cloud fraction (CF), associated with properties such as optical depth, liquid water content, and droplet size distribution, modulates the amount of radiation transmitted to the surface. Additionally, high atmospheric humidity and the presence of aerosols influence the transmissivity of the atmospheric column, introducing variability into GHI and CF signals and increasing the complexity of predictive modeling of these parameters.

In this study, we present a complementary analysis to that described in Rocha et al. (2025), focusing on the relationship between overirradiance, irradiance variability, and cloud cover in Central Amazonia. The seasonal and diurnal characterization of irradiance and cloud fraction was previously discussed in detail in Rocha et al. (2025) and Rocha (2025), and here serves as the basis for investigating the patterns associated with overirradiance events, with emphasis on the contribution of different cloud types and on the temporal scales relevant to photovoltaic operation. The forecasting model employed in this study is described in detail in in the last two works cited and is not reintroduced here, allowing the discussion to concentrate on the meteorological and operational aspects of the events.

1.1. Irradiance variability

One of the most common approaches described in the literature to quantify the short-term variability of surface solar irradiance is through indices based on the ramp concept (Lave et al., 2013). A ramp event, quantified by the metric known as the Ramp Rate (RR), consists of the difference in irradiance between two consecutive time steps and can be characterized by attributes such as magnitude (in irradiance units), duration (in time units), direction (increase or decrease in irradiance), and impulse (ratio between irradiance and time) (Hansen et al., 2010).

With the aim of assessing the availability and stability of the solar resource under different atmospheric conditions, Rocha et al. (2022) present a review of the main indices proposed in the literature for quantifying the variability of GHI. That study employs the Daily Aggregate Ramp Rate (DARR), an index initially introduced by van Haaren et al. (2012), which represents the sum of the absolute values of irradiance variations between consecutive time steps throughout a day, normalized by a constant C = 1000 W/m². In the present work, the differences between these time steps were considered at 1, 2, and 5 minutes. The DARR, whose formulation is presented in Equation 1, enables the quantification of irradiance variability without requiring a clear-sky model as a reference, which constitutes an important practical advantage in terms of applicability.

$$DARR = \sum_{t=1}^{N-1} \frac{|GHI_t - GHI_{t-1}|}{C}$$

(eq. 1)

Furthermore, in Rocha et al. (2022), it is observed that the relationship between solar irradiance and its variability forms an ‘arrowhead’ structure when the clearness index Kt - defined as the ratio between GHI and the irradiance at the Top of Atmosphere (TOA) - is plotted as a function of DARR. This indicates that days with the same mean irradiance level may exhibit very different variability. This result reinforces that magnitudebased metrics, such as GHI or Kt , are not sufficient to infer short-term variability, highlighting the importance of including specific indices such as DARR for a more robust and independent characterization of the solar resource.

1.2. Overirradiance and cloud types

Overirradiance is associated with two main atmospheric mechanisms: cloud enhancement and cloud lensing. In the former case (cloud enhancement), the intensification of global irradiance occurs due to the combination of multiple scattering and reflections between clouds and the surface, resulting in a significant increase in the diffuse component, even under partial cloud cover (Pfister et al., 2003; Thuillier et al., 2013; Gueymard, 2017). Cloud lensing, in turn, is related to the temporary concentration of direct solar radiation at cloud edges, which act as optical lenses, producing transient irradiance peaks that exceed clear-sky values (Balfour, 2011; Zehneret al., 2010). The occurrence of such events is particularly favored under intermediate cloud cover conditions, generally between 50% and 90%, and in scenarios with isolated clouds or well-defined edges (Piacentini et al., 2011).

The morphological and optical properties of clouds play a decisive role in the frequency and intensity of these episodes, as described in Mol and van Heerwaarden (2025). Low *cumulus* clouds, with well-defined edges and strong radiative contrast, are associated with the most intense and variable irradiance peaks. *Altocumulus* clouds, in turn, allow greater direct transmission, enhancing the superposition of direct and diffuse components, whereas *cumulonimbus* clouds tend to block direct irradiance, with localized enhancements occurring only at illuminated edges. *Stratus* and *stratocumulus* clouds, by contrast, exhibit more homogeneous behavior, with low irradiance variability. These structural and optical characteristics explain the predominance of specific cloud types in generating overirradiance observed across different regions and temporal scales.

2. Methodology

The data used in this study were obtained during the GoAmazon 2014/5 experimental campaign (Martin et al., 2016), which investigated the life cycles of aerosols and clouds in Central Amazonia and the effects of urban emissions from Manaus on these atmospheric processes. The T3 site, located in Manacapuru - Amazonas (3.21°S; 60.6°W, UTC–4), was established in a pasture area surrounded by native forest and equipped with instruments designed to measure radiative, hydrological, and meteorological fluxes. The data are publicly available in the ARM (Atmospheric Radiation Measurement) repository (Flynn, 2014; Sengupta et al., 2014). Global horizontal irradiance (GHI) was measured using a ventilated PSP pyranometer from the SKYRAD platform (Andreas et al., 2018), with measurements recorded every 2 seconds and averaged over 1 minute, while CF was obtained from the Total Sky Imager (TSI) (Long et al., 2001), which captures hemispheric sky images every 30 seconds using a heated hemispherical mirror and a movable shadow band to block the solar disk. These images represent local atmospheric conditions at spatial scales of approximately 1 km and temporal scales of up to 30 minutes (Antonanzas et al., 2016).

Cloud type classification was derived from the ARSCL (Active Remote Sensing of Clouds) product (Johnson and Jensen, 1996), which integrates data from multiple active sensors: the W-band cloud radar (WACR), providing vertical profiles of reflectivity; the radar wind profiler (RWP), complementing cloud detection with reflectivity and wind information; the ceilometer (CEIL), identifying up to three cloud-base layers; and the micropulse lidar (MPL), which enhances sensitivity to smaller particles, enabling a more precise characterization of cloud vertical structure. The methodology follows the criteria established by McFarlane et al. (2013) and Burleyson et al. (2015), classifying clouds based on cloud-base height, cloud-top height, and vertical thickness. The product provides a temporal resolution of 30 seconds, vertical information distributed across 600 height levels, and seven cloud classes: Low clouds, *Congestus*, Deep convection, *Altocumulus*, *Altostratus*, *Cirrostratus*/anvil, and *Cirrus*.

3. Results and Discussion

3.1. Variability

The distribution of ramp rate (RR) values exhibits a decreasing asymmetric behavior: a higher concentration of low-magnitude events and a declining frequency as the variation between consecutive time steps increases. This pattern is expected and can be interpreted as resembling a gamma (or exponential) type distribution, since large irradiance ramps (resulting from abrupt atmospheric changes) are naturally rarer compared to small fluctuations.

By contrast, DARR values, as they are obtained from the sum of absolute irradiance differences throughout the day, tend to be distributed more symmetrically around a mean value. This behavior is consistent with an approximately normal (or Gaussian) distribution, resulting from the aggregation of multiple events over time - which, according to the central limit theorem, favors a concentration of values near the mean and a gradual reduction in frequency toward the extremes.

Figure 1 presents the mean ramp size, calculated in cases where GHI values are available for the subsequent minute, across its diurnal cycle using data from the entire study period. A concentration of higher-magnitude ramps and greater variability is observed as solar noon approaches, with a notable afternoon asymmetry in which ramps tend to be slightly more intense. This behavior is associated with the increase in direct irradiance and enhanced cloudiness - as also observed in Rocha (2025). The greater granularity (rapid oscillations between consecutive values) observed in the graph during the peak period may indicate increased cloud variability, with frequent cloud formation and dissipation as well as intermittent shadow passages. These patterns suggest a predominance of short-duration, high-intensity ramps during this interval of the day.

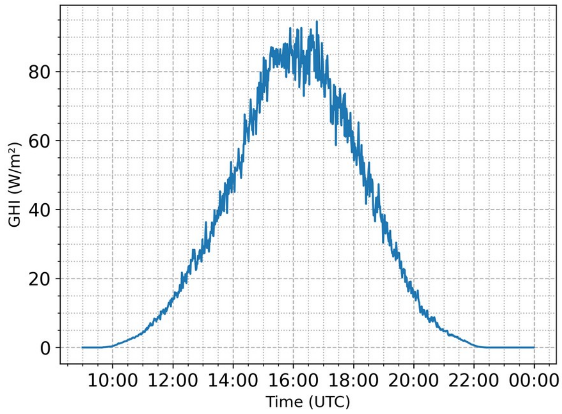

Figure 1: Diurnal cycle of the average irradiance ramps (in W/m²).

Higher DARR values indicate greater irradiance variability, which may be associated with cloud passages. Figure 2 presents the daily and monthly DARR series for three different temporal windows: 1, 2, and 5 minutes. It is observed that the longer the time interval considered between measurements, the lower the mean DARR values (both daily and monthly), and the smaller the dispersion of values. This behavior occurs because the use of longer intervals smooths rapid irradiance fluctuations, reducing the magnitude of instantaneous variations captured and, consequently, the mean DARR values. The fact that 1-minute averages systematically yield higher values than the other intervals indicates that irradiance variations are particularly intense at sub-minute scales.

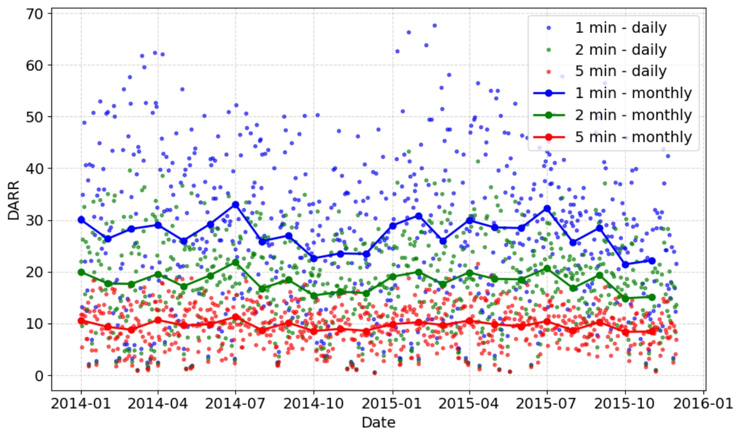

Figure 2: Daily DARR (dots) and monthly averages (lines), with time differences of 1, 2 and 5 minutes (blue, green and red, respectively).

The monthly mean curves exhibit a seasonal pattern, with relatively smooth variations throughout the year. Although the monthly means suggest that July presents the highest DARR values, the analysis of daily values reveals considerable variability across the entire period. This daily dispersion is sufficient to prevent the establishment of a statistically significant conclusion regarding which period exhibits the highest or lowest DARR values. In other words, although the dry season tends to concentrate higher mean values, there are days in other months with variability comparable to or even exceeding that observed in July, making interpretations based solely on means limited. Thus, while the dry season is characterized by higher mean irradiance, this does not imply that daily variability is either lower or higher than in the wet season. Consequently, both in the dry and wet seasons, days with high variability and days with relatively stable conditions may occur.

Considering all 1-minute values (Figure 3), a positive correlation of 0.63 is observed between the DARR index and the daily number of overirradiance events. This value suggests that intraday variability of solar irradiance is associated with the occurrence of such events, and the linear relationship obtained (with a slope of approximately 5) indicates that increases in DARR tend to intensify the frequency of overirradiance events. This result is consistent with the physical behavior of the atmosphere in tropical regions, where the presence of convective clouds and optical effects can induce intense and rapid irradiance fluctuations (Mol and van Heerwaarden, 2025). This observation reinforces that GHI variability acts as a contributing factor to the occurrence of overirradiance, particularly at sub-hourly scales. When considering only values from the wet and dry seasons, the correlation changes to 0.67 and 0.58, respectively. One possible explanation is that greater cloud cover produces more cloud edges, even if mean irradiance is lower, thereby generating numerous smaller oscillations that are more strongly associated with overirradiance events.

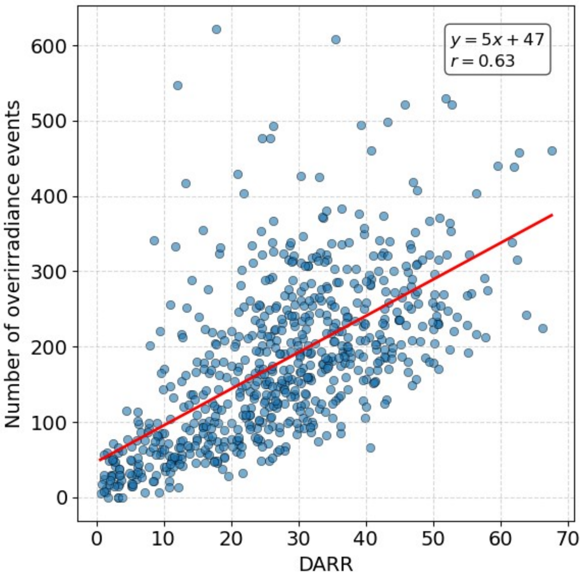

Figure 3: Number of overirradiance events versus DARR, with linear regression line (in red) and respective adjusted equation and Pearson correlation coefficient.

Although the highest mean DARR values occur during the dry season, a stronger correlation is observed between this variability (DARR) and the occurrence of overirradiance events during the wet season. This apparent contradiction can be explained by the different natures of variability in each period: in the dry season, intense ramps associated with isolated clouds against a clear-sky background predominate, which do not always result in overirradiance. In the wet season, the greater coverage of fragmented clouds and the presence of favorable optical conditions (such as cloud edges and multiple scattering) increase the likelihood of overirradiance, even under less intense variability - thereby strengthening the association between DARR and these events during this period. This interpretation is consistent with the hypothesis that, in the study region, the wet season is dominated by larger-scale systems (such as the northwest-to-southeast propagation of South American convection, according to Horel et al. (1989)), whereas the dry season is more strongly influenced by local and isolated convective processes (Machado et al., 2018), which affect cloud structure and the optical mechanisms responsible for overirradiance.

3.2. Cloud types

The analysis of cloud types was conducted using data from the ARSCL product, which provides vertical profiling of cloud cover. Since the data are restricted to the zenith point, they exclusively represent clouds located directly above the sensor, disregarding those inclined toward the horizon. This limitation may introduce significant biases in the analysis, particularly in studies of solar irradiance, as peripheral clouds near the solar disk (often responsible for optical effects associated with overirradiance events) are not adequately represented by vertical profiling. The occurrence of multiple cloud layers (overlap) was not considered in this study, but constitutes a relevant extension for future investigations, given its potential impact on radiative modulation. Such an analysis could be carried out not only with the ARSCL product, which provides vertical profiles, but also with classifications derived from ASIs, which allow observation of cloud cover beyond the zenith point and under different solar geometries.

Figure 4 presents the monthly percentage distribution of the main cloud types observed throughout the study period. Although no marked pattern was identified in the diurnal cycle of the predominant cloud type on each day (not shown), the monthly analysis reveals a significant reduction in the occurrence of vertically developed clouds (such as *cumulus congestus* and deep convective clouds) in 2015 compared to 2014. This difference was particularly pronounced during the dry season, in agreement with the findings of Giangrande et al. (2017). This abrupt change may be related to the configuration of the El Niño phenomenon, even though the event was not fully established in the early months of 2015, combined with large-scale convective forcing during the wet season, which suggests the need for further investigation.

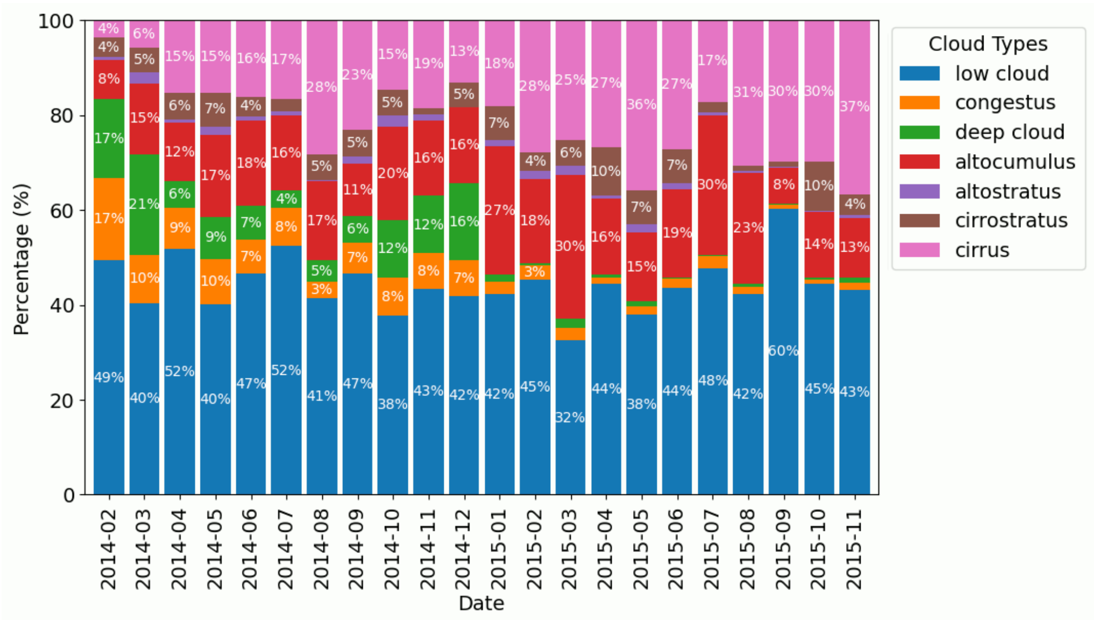

Figure 4: Monthly percentage distribution of the main cloud types observed through the ARSCL product.

An increase in the occurrence of high- and mid-level clouds, such as *cirrus* and *altocumulus*, was observed, particularly during the driest months of 2015, accompanied by a marked reduction in the frequency of vertically developed clouds, such as *cumulus congestus* and deep convective clouds, compared to the previous year. This shift in cloudiness patterns is consistent with a scenario of dry-air subsidence at upper levels, frequently associated with El Niño episodes. The anomalous warming of the eastern Pacific waters alters the Walker circulation, favoring descending motion over the Amazon region. This inhibits the development of deep convective clouds and contributes to the reduction in cloudiness observed during this period. In addition, another factor that may have contributed to this alteration in cloud formation was the significant increase in aerosol concentration in October and November 2015, when aerosol optical depth (AOD) values between 0.4 and 1.0 were recorded (Rocha, 2025). The presence of aerosols can directly and indirectly affect cloud formation and development processes: on the one hand, by scattering and absorbing solar radiation, they reduce surface heating and consequently weaken convection; on the other hand, absorbing aerosols, such as soot from biomass burning, can heat upper atmospheric layers, inducing thermal inversions that hinder vertical cloud growth. This interpretation is consistent with the results of Öktem et al. (2023), who, upon reanalyzing GoAmazon campaign data with objective criteria, found no evidence that aerosols enhance convection intensity in warm-phase clouds, contradicting the strengthening hypothesis and reinforcing the inhibitory role of pollution on vertical cloud development. These changes in atmospheric conditions, including the influence of the ENSO cycle and aerosols, help explain the reduced frequency of deep clouds observed during the second half of 2015.

The diurnal cycle of cloud classification was also examined, identifying the most frequent cloud type for each hour of the day. As the observed pattern was simple and expected, only a textual description is presented. Between 09:00 and 19:00 UTC, low clouds predominate, initially fog and *stratus* clouds, followed by the typical development of diurnal convection in the region. Between 20:00 and 22:00 UTC, the most frequent cloud type shifts to *cirrus*. These observations are consistent with those reported by Giangrande et al. (2017) for the full GoAmazon dataset, identifying the lowest cloud in the column. In the early morning hours, shortly after sunrise, low clouds such as *stratus* or fog prevail, resulting from nocturnal cooling of the near-surface layer, with the nocturnal boundary layer typically between 200 and 250 meters (Carneiro and Fisch, 2020). Subsequently, the typical convective cycle of Central Amazonia develops: during the day, solar heating of the moist surface intensifies convection, forming low *cumulus* clouds, with the top of the Convective Boundary Layer between 1200 and 1400 meters. At the end of the day, as convection weakens and thicker clouds dissipate, ice crystals remain at higher atmospheric levels, favoring the formation of *cirrus*.

Table 1 presents the percentage distribution of cloud types under three distinct conditions: all records with available classification, cases of overirradiance, and cases of overirradiance with GHI greater than 1000 W/m². The “Total” column reflects the mean behavior observed throughout the study period, with a predominance of low clouds, followed by *cirrus* and *altocumulus* - a pattern consistent with the typical convective cycle of Central Amazonia.

Table 1: Percentage distribution of cloud types in three different conditions: all data with cloud classification, only cases with overirradiance (OI), and overirradiance with GHI greater than 1000 W/m² (OI c /GHI>1000), in percentages.

Cloud type	Total	OI	OI (GHI>1000)
1 - Low cloud	44	50	78
2 - *Congestus*	6	2	1
3 - Deep cloud	7	0	1
4 - *Altocumulus*	17	21	12
5 - *Altostratus*	1	1	0
6 - *Cirrostratus*	5	2	1
7 - *Cirrus*	20	25	7

When restricting the data to instances of overirradiance, an amplification of disparities among cloud types is observed: low clouds, *altocumulus*, and *cirrus* become more frequent, while congestus and deep convective clouds show reduced occurrence. This asymmetry suggests that certain cloud types are more prone to generating overirradiance. Low *cumulus* clouds, for example, exhibit well-defined edges that enhance scattering and focusing of sunlight, amplifying irradiance at the surface. High *cirrus* clouds, composed of ice crystals, may act as optical lenses, concentrating sunlight at specific angles—albeit with lower efficiency (Balfour, 2011).

When the additional criterion of GHI > 1000 W/m² is applied, the dominance of low clouds becomes even more evident, representing 78% of cases, while all other types significantly reduce their contribution. This extreme subset imposes a condition of very high irradiance, which can only be achieved under highly specific optical conditions—generally associated with partly cloudy skies and low convective clouds near the solar disk. In such situations, solar geometry favors the occurrence of refraction and directed reflection effects, which are more likely with clouds close to the surface due to the more favorable incidence angle.

It is important to note that the reduced participation of congestus and deep convective clouds in overirradiance events may be related to a limitation of the observation method, since cloud types are identified based on zenithal vertical profiling. Thus, events generated by clouds inclined or peripheral to the solar disk may not be adequately captured, even though they have the potential to produce intense increases in measured irradiance. Nevertheless, the results reinforce the importance of low clouds in the generation of overirradiance, particularly under conditions of high direct irradiance.

To investigate the relationship between cloud types and the intensity of irradiance ramps, the dataset was filtered to include only cases in which the absolute variation between two consecutive GHI values was greater than or equal to 100 W/m². This choice is justified by the fact that approximately 88% of the observed ramps have magnitudes below this threshold, so that focusing on the most intense ramps allows the analysis to concentrate on variations with greater impact for energy and operational applications, since oscillations of this magnitude may compromise the real-time stability of solar systems, requiring enhanced response capacity. Figure 5 presents the distribution of these ramps for each cloud type, based on classifications obtained from vertical profiling.

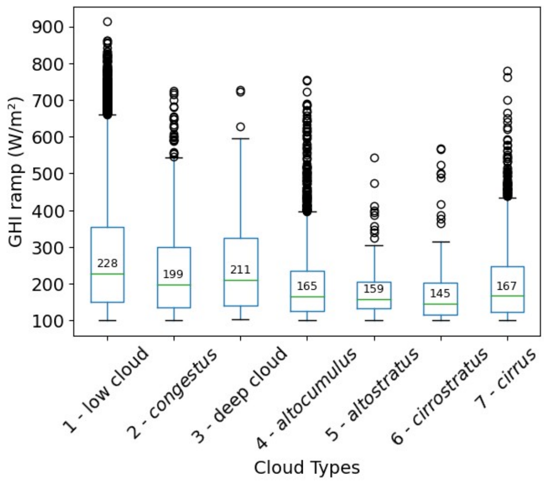

Figure 5: Distribution of global solar irradiance (GHI) slopes with a module greater than or equal to 100 W/m² for each cloud type, with the median values written in the respective boxes.

The marked presence of outliers in the distributions of GHI ramps associated with cloud types such as low clouds (sample size n = 21,391), *altocumulus* (n = 2,634), *cirrus* (n = 1,430), and *congestus* (n = 573) suggests that these formations are linked to a higher occurrence of abrupt irradiance ramps, possibly due to their fragmented structure, short duration, or strong vertical dynamics. Lower clouds (categories 1 to 3) tend to exhibit ramps of greater magnitude and variability, with medians slightly above 200 W/m². This behavior is attributable to their higher optical thickness and proximity to the surface, which produce more abrupt shadowing as they move across the measurement point. Low clouds and congestus are particularly associated with intense ramps, given their opacity and atmospheric dynamics.

By contrast, cloud types such as deep convection (n = 70), *altostratus* (n = 93), and *cirrostratus* (n = 127) presented fewer samples and fewer outliers, which may reflect both more homogeneous and persistent physical characteristics (inhibiting rapid irradiance transitions) and the statistical effect of reduced sampling. These analyses highlight the importance of considering not only cloud type, but also intra-class variability and the role of factors such as solar geometry and the local dynamics of the cloud–radiation system.

4. Conclusions

The variability of GHI, quantified by the DARR index, is positively associated with the occurrence of overirradiance events, with an overall correlation of 0.63. This relationship is stronger during the wet season (r = 0.67) than in the dry season (r = 0.58), indicating that the fragmented structure of clouds and the optical conditions present during the wet season favor the occurrence of rapid fluctuations capable of generating overirradiance. The seasonal analysis of DARR indicated greater variability in the dry season, particularly in July, which can be attributed to the combination of high direct irradiance with isolated *cumulus* clouds. The higher intraday variability and the concentration of intense ramps around solar noon, especially with an afternoon asymmetry, suggest that this is the period most susceptible to rapid and intense oscillations. Furthermore, the fact that mean DARR values decrease with increasing temporal window confirms that very short-term variability is relevant for characterizing atmospheric instability.

The analysis of cloud types revealed distinct patterns at seasonal, diurnal, and event-specific scales. In 2015, a marked reduction was observed in the occurrence of vertically developed clouds (such as *cumulus congestus* and deep convection), possibly associated with El Niño and with aerosols, which inhibited vertical cloud development. The diurnal cycle indicates a predominance of low clouds between 09:00 and 19:00 UTC, with *cirrus* dominating at night, reflecting the typical convective development of Central Amazonia. During overirradiance events, especially under GHI > 1000 W/m², low clouds predominate; due to their geometry and optical thickness, they favor mechanisms of solar light concentration and scattering. *Cirrus* and *altocumulus* also increase their frequency in such events, although with lower optical efficiency. The reduced occurrence of deep clouds in these episodes may result from methodological limitations related to zenithal profiling, which does not capture clouds in geometries more favorable to overirradiance. In the analysis of intense ramps (greater than 100 W/m²), low clouds and *cumulus congestus* exhibit higher magnitudes and variability, with abrupt shadowing associated with their opacity and proximity to the surface. Conversely, high clouds such as *cirrus* generate less intense ramps, though still with the presence of outliers, indicating that the intensity of irradiance variations depends not only on cloud type but also on intra-class variability and the interaction with solar geometry and local atmospheric dynamics.

Detailed characterization of the relationship between irradiance variability, overirradiance, and cloud types provides direct insights for improving very short-term forecasting models, especially those based on machine learning. This approach was explored in the work described in Rocha et al. (2025) and Rocha (2025), which integrates the physical aspects discussed here into the development of predictive models.

5. Acknowledgments

This study was financed in part by the Coordenação de Aperfeiçoamento de Pessoal de Nível Superior - Brasil (CAPES) - Finance Code 001, process n. 88887.885659/2023-00, and process n. 88887.601400/2021-00. The authors are also grateful for the funding received through the projects "Evaluation of the photovoltaic resource in hydroelectric reservoirs based on numerical modeling and remote sensing" (CNPq 409711/2021-7), INCT-Mudanças Climáticas Fase 2 (FAPESP 2014/50848-9, CNPq 465501/2014-1, CAPES/FAPS No 16/2014) and FINEP SOLTER - "Union by Diffusion of Light Metals in Compact Solar Energy Storage Devices for Electricity Generation from Solar Thermal Sources in Brazil” (FINEP 0018/21). António Ruano wishes to acknowledge the support of Fundação para a Ciência e a Tecnologia (FCT) for its financial support via the project LAETA Base Funding (DOI: 10.54499/UIDB/50022/2020).

6. References

ABSOLAR, 2025. Infográfico — Associação Brasileira de Energia Solar Fotovoltaica. URL: https://www.absolar.org.br/mercado/infografico/. Last access: 2025-07-02.

Andreas, A., Dooraghi, M., Habte, A., Kutchenreiter, M., Reda, I., Sengupta, M., 2018. Solar Infrared Radia-tion Station (SIRS), Sky Radiation (SKYRAD), Ground Radiation (GNDRAD), and Broadband Radiometer Station (BRS) Instrument Handbook. National Renewable Energy Laboratory (NREL) - U.S. Department of Energy (DOE). doi:10.2172/1432706.

Antonanzas, J., Osorio, N., Escobar, R., Urraca, R., de Pison, F.M., Antonanzas-Torres, F., 2016. Review of photovoltaic power forecasting. Solar Energy 136, 78–111. doi:10.1016/j.solener.2016.06.069.

Balfour, J., 2011. Introduction to photovoltaic installations. Jones & Bartlett Learning. URL: https://books.google.com.br/books?id=Lje9wAEACAAJ. Burleyson, C.D., Long, C.N., Comstock, J.M., 2015. Quantifying diurnal cloud radiative effects by cloud type in the tropical western pacific. Journal of Applied Meteorology and Climatology 54, 1297–1312. doi:10.1175/jamc-d-14-0288.1.

Carneiro, R.G., Fisch, G., 2020. Observational analysis of the daily cycle of the planetary boundary layer in the central Amazon during a non-El Niño year and El Niño year (GoAmazon project 2014/5). Atmospheric Chemistry and Physics 20, 5547–5558. doi:10.5194/acp-20-5547-2020.

Flynn, D., 2014. Total sky imager (tsiskycover), 2014-01-01 to 2015-12-01, arm mobile facility (mao), manacapuru, amazonas, brazil; amf1 (m1). doi:10.5439/1992207.

Giangrande, S.E., Feng, Z., Jensen, M.P., Comstock, J.M., Johnson, K.L., Toto, T., Wang, M., Burleyson, C., Bharadwaj, N., Mei, F., Machado, L.A.T., Manzi, A.O., Xie, S., Tang, S., Dias, M.A.F.S., de Souza, R.A.F., Schumacher, C., Martin, S.T., 2017. Cloud characteristics, thermodynamic controls and radiative impacts during the observations and modeling of the Green Ocean Amazon (GoAmazon2014/5) experiment. Atmospheric Chemistry and Physics 17, 14519–14541. doi:10.5194/acp-17-14519-2017.

Gueymard, C.A., 2017. Cloud and albedo enhancement impacts on solar irradiance using high-frequency measurements from thermopile and photodiode radiometers. part 1: impacts on global horizontal irradiance. Solar Energy 153, 755–765. doi:10.1016/j.solener.2017.05.004.

van Haaren, R., Morjaria, M., Fthenakis, V., 2012. Empirical assessment of short-term variability from utility scale solar pv plants. Progress in Photovoltaics: Research and Applications 22, 548–559. doi:10.1002/pip.2302.

Hansen, C.W., Stein, J.S., Ellis, A., 2010. Statistical criteria for characterizing irradiance time series. Technical Report SAND2010-7314. Sandia National Laboratories. Albuquerque, NM, USA.

Horel, J.D., Hahmann, A.N., Geisler, J.E., 1989. An investigation of the annual cycle of convective activity over the tropical americas. Journal of Climate 2, 1388–1403. doi:10.1175/1520-0442(1989)002<1388:aiotac>2.0.co;2.

Johnson, K., Jensen, M., 1996. Arm: Arscl: multiple outputs from first clothiaux algorithms on vaisala or belfort ceilometers, micropulse lidar, and mmcr. doi:10.5439/1027282.

Laing, A.G., Evans, J.L., 2011. Challenges of tropical weather forecasting, in: Introduction to Tropical Meteorology. 2 ed.. COMET Program, University Corporation for Atmospheric Research (UCAR). chapter 9.1.

Lave, M., Kleissl, J., Ellis, A., Mejia, F., 2013. Simulated pv power plant variability: impact of utility-imposed ramp limitations in puerto rico, in: Proceedings..., IEEE Photovoltaic Specialists Conference. IEEE. pp. 1817–1821. doi:10.1109/pvsc.2013.6744495.

Long, C.N., Slater, D.W., Tooman, T., 2001. Total Sky Imager (TSI) model 880 status and testing results. Technical Report ARM TR-006. U.S. Department of Energy, Atmospheric Radiation Measurement Program. Washington, D.C. URL: http://www.arm.gov/docs/documents/techpreports/index.html.

Machado, L.A.T., Calheiros, A.J.P., Biscaro, T., Giangrande, S., Dias, M.A.F.S., Cecchini, M.A., Albrecht, R., Andreae, M.O., Araujo, W.F., Artaxo, P., Borrmann, S., Braga, R., Burleyson, C., Eichholz, C.W., Fan, J., Feng, Z., Fisch, G.F., Jensen, M.P., Martin, S.T., Pöschl, U., Pöhlker, C., Pöhlker, M.L., Ribaud, J.F., Rosenfeld, D., Saraiva, J.M.B., Schumacher, C., Thalman, R., Walter, D., Wendisch, M., 2018. Overview: precipitation characteristics and sensitivities to environmental conditions during GoAmazon2014/5 and ACRIDICON-CHUVA. Atmospheric Chemistry and Physics 18, 6461–6482. doi:10.5194/acp-18-6461-2018.

Martin, S.T., Artaxo, P., Machado, L.A.T., Manzi, A.O., Souza, R.A.F., Schumacher, C., Wang, J., Andreae, M.O., Barbosa, H.M.J., Fan, J., Fisch, G., Goldstein, A.H., Guenther, A., Jimenez, J.L., Pöschl, U., Dias, M.A.S., Smith, J.N., Wendisch, M., 2016. Introduction: observations and modeling of the Green Ocean Amazon (GoAmazon2014/5). Atmospheric Chemistry and Physics 16, 4785–4797. doi:10.5194/acp-16-4785-2016.

McFarlane, S.A., Long, C.N., Flaherty, J., 2013. A climatology of surface cloud radiative effects at the arm tropical western pacific sites. Journal of Applied Meteorology and Climatology 52, 996 – 1013. doi:10.1175/JAMC-D-12-0189.1.

Mol, W., van Heerwaarden, C., 2025. Mechanisms of surface solar irradiance variability under broken clouds. Atmospheric Chemistry and Physics 25, 4419–4441. doi:10.5194/acp-25-4419-2025.

Öktem, R., Romps, D.M., Varble, A.C., 2023. No warm-phase invigoration of convection detected during goamazon. Journal of the Atmospheric Sciences 80, 2345–2364. doi:10.1175/jas-d-22-0241.1.

Pereira, E., Martins, F., Gonçalves, A., Costa, R., Lima, F., Rüther, R., Abreu, S., Tiepolo, G., Pereira, S., Souza, J., 2017. Atlas brasileiro de energia solar. Universidade Federal de São Paulo. doi:10.34024/978851700089.

Pfister, G., McKenzie, R.L., Liley, J.B., Thomas, A., Forgan, B.W., Long, C.N., 2003. Cloud coverage based on all-sky imaging and its impact on surface solar irradiance. Journal of Applied Meteorology 42, 1421 – 1434. doi:10.1175/1520-0450(2003)042<1421:CCBOAI>2.0.CO;2.

Piacentini, R.D., Salum, G.M., Fraidenraich, N., Tiba, C., 2011. Extreme total solar irradiance due to cloud enhancement at sea level of the ne atlantic coast of brazil. Renewable Energy 36, 409–412. doi:10.1016/j.renene.2010.06.009.

REN21, 2025. Renewables Global Status report. URL: https://www.ren21.net/reports/global-status-report/.

Rocha, V.R.d., 2025. Previsão de irradiância e sobreirradiância na Amazônia com aprendizado de máquina. Ph.D. thesis. Instituto Nacional de Pesquisas Espaciais. São José dos Campos.

Rocha, V.R.d., Costa, R.S., Martins, F.R., Gonçalves, A.R., Pereira, E.B., 2022. Variability index of solar resource based on data from surface and satellite. Renewable Energy 201, 354–378. doi:10.1016/j.renene.2022.10.093.

Rocha, V.R.d., Fisch, G., Costa, R.S., Martins, F.R., Gonçalves, A.R., Ruano, A., 2025. Forecasting irradiance and overirradiance in the amazon: A machine learning and event characterization study. SSRN Electronic Journal doi:10.2139/ssrn.5352185.

Sengupta, M., Habte, A., Andreas, A., Reda, I., Jaker, S., Xie, Y., Yang, J., Gotseff, P., Kutchenreiter, M., Shi, Y., 2014. Sky radiometers on stand for downwelling radiation (skyrad60s), 2014-01-01 to 2015-12-01, arm mobile facility (mao), manacapuru, amazonas, brazil; amf1 (m1). Doi:10.5439/1377836.

Thuillier, G., Perrin, J.M., Keckhut, P.L., Huppert, F., 2013. Local enhanced solar irradiance on the ground generated by cirrus: measurements and interpretation. Journal of Applied Remote Sensing 7, 073543. doi:10.1117/1.JRS.7.073543.

Zehner, M., Hartmann, M., Weizenbeck, J., Gratzl, T., Weigl, T., Mayer, B., Wirth, G., Krawczynski, M., Betts, T., Gottschalg, R., Hammer, A., Giesler, B., Becker, G., Mayer, O., 2010. Systematic analysis of meteorological irradiation effects, in: Proceedings..., Photovoltaic Solar Energy Conference, Valencia, Spain. pp. 6–10.